Ultrasound in Med. & Biol., Vol. 28, No. 10, pp. 1301–1310, 2002

0301-5629/02/$–see front matter

PII: S0301-5629(02)00620-8

● *Original Contribution*

DIAGNOSIS OF BREAST TUMORS WITH SONOGRAPHIC TEXTURE ANALYSIS USING WAVELET TRANSFORM AND NEURAL NETWORKS

DAR-REN CHEN,* RUEY-FENG CHANG,† WEN-JIA KUO,† MING-CHUN CHEN† and YU-LEN HUANG†

*Department of General Surgery, China Medical College & Hospital, Taichung, Taiwan; and †Department of Computer Science and Information Engineering, National Chung Cheng University, Chiayi, Taiwan

(*Received* 28 *February* 2002; *in final form* 30 *July* 2002)

Abstract—To increase the ability of ultrasonographic technology for the differential diagnosis of solid breast tumors, we describe a novel computer-aided diagnosis (CADx) system using neural networks for classification of breast tumors. Tumor regions and surrounding tissues are segmented from the physician-located region-of-interest (ROI) images by applying our proposed segmentation algorithm. Cooperating with the segmentation algorithm, three feasible features, including variance contrast, autocorrelation contrast and distribution distortion of wavelet coefficients, were extracted from the ROI images for further classification. A multilayered perceptron (MLP) neural network trained using error back-propagation algorithm with momentum was then used for the differential diagnosis of breast tumors on sonograms. In the experiment, 242 cases (including benign breast tumors from 161 patients and carcinomas from 82 patients) were sampled with *k*-fold cross-validation ($k = 10$) to evaluate the performance. The receiver operating characteristic (ROC) area index for the proposed CADx system is 0.9396 ± 0.0183, the sensitivity is 98.77%, the specificity is 81.37%, the positive predictive value is 72.73% and the negative predictive value is 99.24%. Experimental results showed that our diagnosis model performed very well for breast tumor diagnosis. (E-mail: dlchen88@ms13.hinet.net) © **2002 World Federation for Ultrasound in Medicine & Biology.**

Key Words: **Ultrasonic, Breast tumor, Wavelet transform, Neural network.**

INTRODUCTION

Breast cancer is the most prevalent cancer among women, and has become the leading cause of cancer deaths among women 15 to 54 years old (Boring et al. 1994; Sahiner et al. 1996). The best way to reduce cancer deaths due to breast cancer is early detection and treatment. Currently, self-examination, mammography and sonography are the most frequently adopted methods for early detection of breast cancers. Despite the existence of many kinds of detection methodologies, the best way accurately to differentiate whether the tumor is benign or malignant is biopsy. In comparison with other procedures, biopsy is very expensive for the large number of indeterminate lesions that need to be differentiated per year. Therefore, it becomes constructive to diminish invasive methods of distinguishing malignant from benign masses of the breast to reduce the number of unnecessary biopsies, allay anxiety and control costs. Mammography and sonography are supplied in most hospitals for doctors to diagnose *via* visual experiences. Biopsy is usually performed under the condition when suggested by doctors. Nevertheless, most biopsies are avoidable because the rate of positive findings at biopsy for cancers is low, between 10% and 31% (Bassett et al. 1993; Gisvold and Martin 1984; Rosenberg et al. 1987). Therefore, many researchers have investigated CADx systems that support objective evidence with high differential rates.

A CADx system could assist inexperienced physicans to avoid misdiagnoses, reduce the number of benign lesion biopsies without missing cancers, and decrease the variations of various observers. Currently, both mammograms (Dhawan et al. 1996; Petrick et al. 1996; Sahiner et al. 1996; Zheng et al. 1996; Jiang et al. 2001; Freer and Ulissey 2001) and sonograms (Shankar et al. 1993; Chou et al. 2001) can be digitized to cooperate with a CADx system. Although the nonpalpable and minimal tumors can be detected by mammography, sonography is still suitable for palpable tumors. Furthermore, sonography

Address correspondence to: Dr. Dar-Ren Chen, Department of General Surgery, China Medical College & Hospital, 2 Yer-Der Rd, Taichung, Taiwan. E-mail: dlchen88@ms13.hinet.net

has been shown to be similar in overall effectiveness to the use of mammography, and even better than mammography for women less than 35 years old. In the report by Stavros et al. (1995), the promising results of breast ultrasound (US) for the classification of benign from malignant cases were obtained using several observer features. This study sparked both a renewed interest in expanding the role of breast US and controversy over the experimental approach necessary to prove the independent value of sonography. However, using these descriptors by Stavros and colleagues may require real-time evaluation by an experienced interpreter. Furthermore, the interobserver variations in the interpretation of sonographic findings were unavoidable. Garra et al. (1993) suggested that it could notably reduce the number of benign biopsies of the breast through analyzing the sonographic textures. Texture is known to provide cues about scenic depth and surface orientation. Texture is a rich source of visual information and is a key component in image analysis.

Wavelet transform has been identified as a good technique for the representation of time-frequency signals (Antonini et al. 1992; Averbuch et al. 1996; Chang and Kao 1993; Mallat 1989a). One of the ways to perform wavelet transform is similar to using the quadrature mirror filter (QMF) banks in subband coding, and several decomposition levels are cascaded into a pyramidal structure. With the properties of reserving local texture complexity, the wavelet transform can be applied to extract local texture features and to detect multiresolution characteristics, especially in image-processing applications. It has also been applied in many image techniques, such as feature enhancement, texture discrimination, texture segmentation, pattern recognition, data compression, teleradiology and image acquisition (Richardson 1995). Thus, the wavelet coefficients played an important role in our segmentation algorithm for segmenting the tumors in ultrasonic breast images. Meanwhile, the distribution of wavelet coefficients can be utilized for differentiating malignant cases from benign cases, because local texture characteristics are well reinforced by wavelet transform.

The neural network is a model that simulates the human learning process. Recently, it has been applied in many discriminating systems with good performance, such as pattern recognition, voice recognition and optical character reading. In the researches of differentiating breast tumors, the neural network has also been successfully applied to detect microcalcifications in digital mammographic images (Dhawan et al. 1996; Sahiner et al. 1996; Zheng et al. 1996). Therefore, the neural network with error backpropagation algorithm proposed by Rumelhart et al. (1986) and Hirose et al. (1991) was adopted as our discriminating technique. In addition, three feasible features are proposed as the inputs to the neural network to differentiate malignant from benign cases. The overall performance of our proposed method is also compared with the standard linear classifier (Therrien 1989).

MATERIALS AND METHODS

In the past few years, wavelet transforms and neural networks have been successfully used in many applications. In this section, we briefly introduce these two techniques mainly used in this study.

Wavelet transform

The wavelet bases $\psi(x)$ are functions generated from a kernel function $\Psi(x)$ called the mother wavelet, by dilation and translation as follows:

$$\psi_{2^s,t}(x) = \psi_{2^s}(x - 2^{-s}t) = 2^s\Psi(2^s x - t), \qquad (1)$$

where s and t are dilation and translation parameters. The mother wavelet $\Psi(x)$ must satisfy the condition that either:

$$\int \Psi(x)dx = 0, \qquad (2)$$

or

$$\int \frac{|\hat{\Psi}(w)|^2}{|w|}\,dw < \infty, \qquad (3)$$

where $\hat{\Psi}(w)$ is the Fourier transform of $\Psi(x)$. Wavelet decomposition is performed by convolving the signal $f(x)$ with the wavelet bases $\psi(x)$; that is,

$$\langle f(x),\ \psi_{2^s,t}(x)\rangle = \int f(x)\psi_{2^s,t}(x)dx. \qquad (4)$$

Many different wavelet bases have been constructed and correspond to multiresolution analyses (Antonini et al. 1992). In multiresolution analysis, let $\varphi(x)$ and $\Psi(x)$ be the scaling function and associated mother wavelet; the computation of $\langle f(x),\varphi_{2^s,t}(x)\rangle$ is then formulated as follows:

$$\langle f(x),\varphi_{2^{s+1},t}(x)\rangle = \sum_k h(k - 2t)\langle f(x),\ \varphi_{2^s,k}(x)\rangle. \qquad (5)$$

and

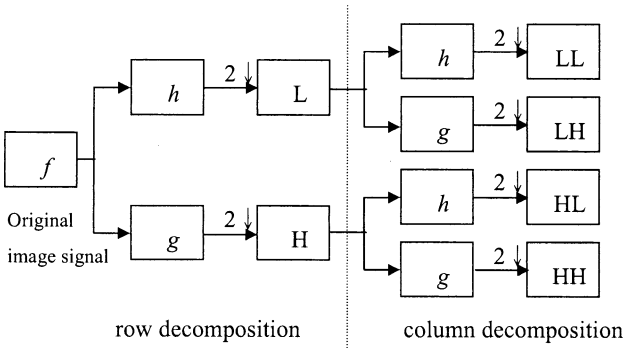

Fig. 1. An example of 2-D representation of the wavelet decomposition.

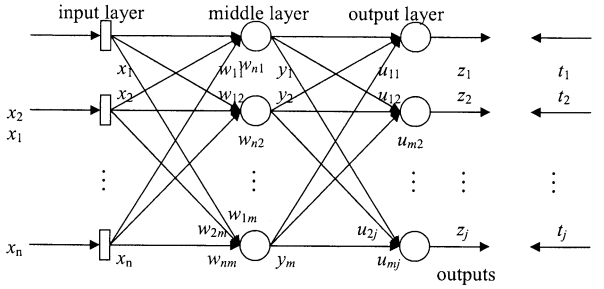

Fig. 2. A model of multilayered perception (MLP) neural network.

$$\langle f(x), \psi_{2^{s+1},t}(x)\rangle = \sum_k g(k-2t)\langle f(x), \varphi_{2^s,k}(x)\rangle, \quad (6)$$

where $h(t) = \langle \varphi_{2^{s+1}}, \varphi_{2^s,t}\rangle$ is a low-pass filter, $g(t) = \langle \psi_{2^{s+1}}, \varphi_{2,^s t}\rangle$ is a high-pass filter and $g(t) = (-1)^t h(1-t)$. We could find that $\langle f(x), \varphi(x)\rangle$ at 2^{S+1} scale could be achieved by passing $\langle f(x), \varphi(x)\rangle$ at 2^S scale through the low-pass filter $h(t)$. Similarly, we could find that $\langle f(x), \psi(x)\rangle$ at 2^{S+1} scale could be achieved by passing $\langle f(x), \varphi(x)\rangle$ at 2^S scale through high-pass filter $g(t)$.

On the other hand, to reconstruct $f(x)$ at 2^S scale, $\langle f(x), \varphi_{2^s,t}(x)\rangle$ is defined as:

$$\langle f(x), \varphi_{2^s,t}(x)\rangle = \sum_t (\bar{h}(k-2t)\langle f(x), \varphi_{2^{s+1},t}(x)\rangle + \bar{g}(k-2t)\langle f(x), \psi_{2^{s+1},t}(x)\rangle), \quad (7)$$

where $\bar{h}(t)$ and $\bar{g}(t)$ are the associated reconstruction pair of $h(t)$ and $g(t)$. We could find that the reconstruction of $f(x)$ at 2^S scale could be achieved by summing the results after low-pass filtering and high-pass filtering the signal at 2^{S+1} level from the previous decomposition stage. If the wavelet bases are orthogonal, then we could achieve an exact reconstruction by setting $h(t) = \bar{h}(t)$, and $g(t) = \bar{g}(t)$. If the fast computation is expected, the biorthogonal decomposition bases can be used to achieve the exact reconstruction by setting $\bar{g}(t) = (-1)^t h(1-t)$ and $g(t) = (-1)^t \bar{h}(1-t)$.

A 2-D subband filter scheme is used when applying the wavelet transform for image applications. Figure 1 depicts an example of the 2-D subband scheme. First, a 1-D decomposition filter is applied to each row of the image signal and then two filtered subimages, L and H, are generated by down-sampling. The size of each subimage is half of the original image size. The same 1-D decomposition filter is applied to each column of subimages L and H, and four subimages, LL, LH, HL and HH, are generated by down-sampling. The size of each subimage is one quarter of the original image size.

Neural networks

A neural network is a model that simulates the functions of biologic neurons. The ability of a single neuron could be greatly improved by connecting multiple neurons in a layered network called MLP or feed-forward artificial neural network, as shown in Fig. 2. The first layer is the input layer that receives input vectors. Each neuron in the hidden layer and output layer receives output vectors of their previous layer to evaluate the weighted sum of vectors and, then, to achieve the output vectors by the activation functions of the neurons.

The main goal of an image-recognition system using neural networks is to achieve the purpose that evaluates the input signals to the desired outputs correctly. If the input feature vectors are chosen properly, a well-trained MLP neural network will achieve good performance for image recognition by its nonlinear, stable and high-dimensional segmentation properties.

In this section, we describe our proposed method for diagnosis of breast tumors in sonographic images.

Segmentation of tumors from the ROI image

An ROI image is an appropriate image containing the important contents in which we are interested. Especially, it is more useful to make use of the ROI images for medical image processing. An example of the ROI image selected for tumor diagnosis is shown in Fig. 3. We can find that the tumor is obviously exhibited in the central region of the image. For the ROI image, it is clear that color, brightness and texture characteristics of the tumor are apparently distinguishable from those of surrounding healthy tissues. However, there still exists a considerable number of nontumor regions around the tumor in an ROI image. In this case, the result would reduce the accuracy rate of diagnosis for CADx systems. Therefore, we propose a segmentation method for the

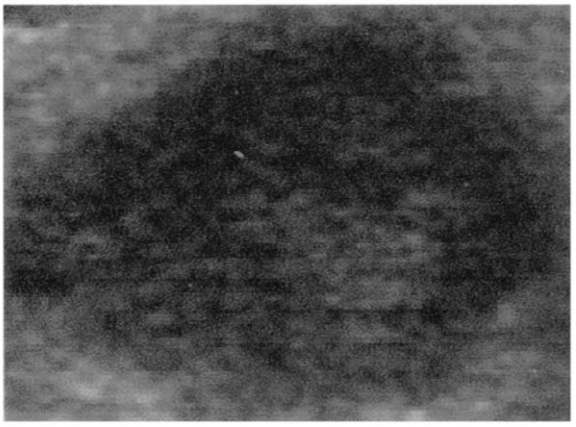

Fig. 3. An ROI image.

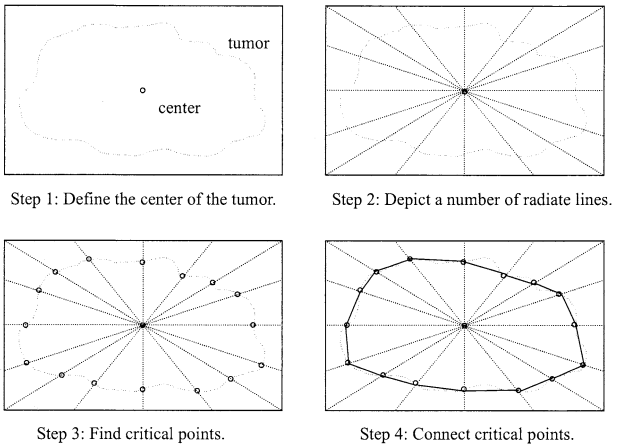

Fig. 4. The segmentation algorithm to segment the tumor from surrounding tissues.

purpose of removing the nontumor regions from an ROI image.

The segmentation algorithm applied in the ROI images to segment the tumor is described as follows.

Step 1: For the reason that an ROI image of a tumor is selected by physician, the center of the tumor is expected to approximate the center of the ROI image. Hence, we assume that the center of the ROI image is the center of the tumor.

Step 2: A number of radial lines are depicted from the approximated center of the tumor defined previously to the boundary of the ROI image.

Step 3: Along with each radial line, we find a critical point that approximates the boundary of the tumor and surrounding tissues.

Step 4: Finally, the critical points of the adjacent radial lines are connected to depict the contour of the tumor.

Figure 4 clearly shows an illustration of the segmentation algorithm.

The major difficulty of the proposed segmentation algorithm is the way of finding the critical points along with the radial lines at step 3. We describe the method of detecting critical points as follows.

Step 1: Apply the wavelet transform on ROI image to obtain four subband images.

Step 2: For the LL and HL subband images, evaluate the associated local variance for each pixel by sliding a variance-evaluating window throughout the whole image. The local variance is defined so as to evaluate the variance in a predefined $m \times n$ rectangle with the currently processed pixel in the center.

Step 3: Scan the pixels along with the radial line from the center of the tumor to the image boundary to find the pixel whose local variance in LL or HL subband is maximal. The maximum pixel is then considered the most likely boundary point of the tumor because of its high local variance. One thing we should note carefully is that we must avoid some nonboundary high-complexity areas inside the tumor being misjudged as boundary points. To avoid such misjudgment, we make some modifications during the scanning procedure. If there exists a pixel scanned after the currently found maximum point whose local mean is larger than the average of all local means and local variance is greater than average of all local variance, the pixel is then considered still to be inside the tumor. This inside point is defined as the new maximum point and the scanning procedure continuously works for the pixels in the radial line. Figure 5 shows an example of finding the critical point of the tumor.

Step 4: After scanning all the pixels in the radial line, the maximum point is considered to be the critical point of this radial line.

The main reason we adopt wavelet transform for the segmentation procedure is that wavelet transform could reinforce local characteristics of textures, and the local variance of wavelet coefficients is useful to extract local

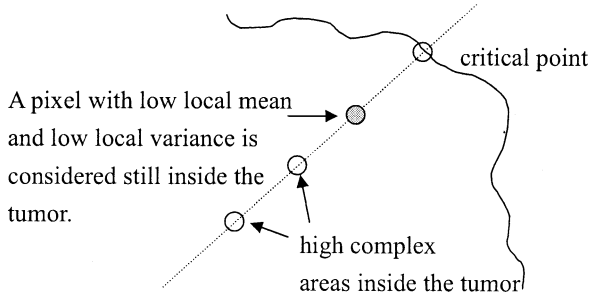

Fig. 5. Finding the boundary of the tumor.

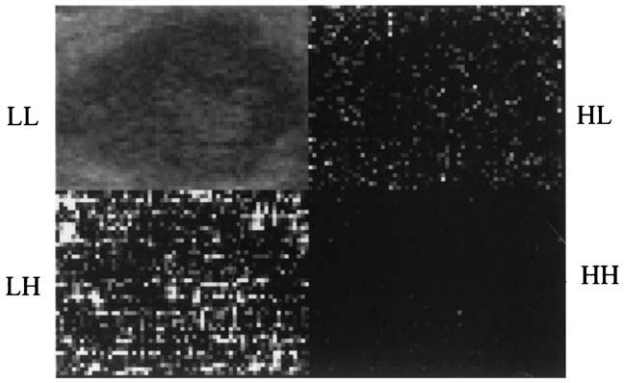

Fig. 6. The four subbands of an ROI image for Fig. 3.

texture characteristics. Meanwhile, the local texture characteristics are the most important properties to differentiate two different regions in an image. In our method, the LH subband is not used because of massive noise and the HH subband is also not used because signals are weak and ambiguous. Figure 6 shows the four subband images of the ROI image shown in Fig. 3.

Feasible features for diagnosis

To differentiate the benign and malignant breast tumors in the sonograms effectively, it is not enough to make use of the most traditional texture properties such as mean, variance, skewness and energy in the discriminating procedure. The main reason is that these texture properties contains information for the global texture, but ignore local texture properties. Hence, in this paper, we propose three feasible features, including variance contrast, autocorrelation contrast and distribution distortions of wavelet coefficients, to increase the ability of diagnosis. Both of the variance contrast and autocorrelation contrast are constructed with the segmentation algorithm and the distribution distortion of wavelet coefficients is extracted from the HL subband of the ROI image. We introduce these three features as follows.

Variance contrast

Because we have segmented the tumor region from the surrounding tissues, the original image could be divided into two regions: inside region (the tumor) and outside region (the surrounding tissue). The variance contrast is defined as the ratio of variance of the inside region and variance of the outside region. The variance of a region is defined as:

$$\sigma = \frac{\sum_{i=1}^{N}(x_i - \bar{x})^2}{N}, \tag{8}$$

where $x|Az$ is the mean value of the region and N is the number of pixels in the region. Thus, the variance contrast can be written as $\sigma_{\text{inside}}/\sigma_{\text{outside}}$.

Autocorrelation contrast

Many researches in US texture analysis had been proposed over the last 20 years. The natural textures usually have a highly stochastic characterization, whether they are structured or not. It would seem advisable to use statistical measurements to characterize those signals that are insufficiently described by most other approaches. Statistical parameters are evaluated either at order one, at order two or at higher orders.

The most useful features were those directed from co-occurrence matrices of the image described as follows.

A co-occurrence matrix, $P_{\phi,d}(i, j)$, is a matrix where the (i,j)th element describes the frequency of occurrence of two pixels that are separated by distance d in the direction ϕ with grey levels i and j. For an $N \times N$ region with M grey levels $(0, \ldots, M-1)$, the grey-level differences that single pairs of pixels can exhibit are:

$$\begin{matrix} (0,0) & (0,1) & \ldots & (0,M-1) \\ (1,0) & (1,1) & \ldots & (1,M-1) \\ \vdots & \vdots & \vdots & \vdots \\ (M-1,0) & (M-1,1) & \ldots & (M-1,M-1) \end{matrix}$$

We can find that the co-occurrence matrix can capture the texture variations in a region by various ϕ and d. The main power of the co-occurrence matrix approach is that it characterizes the spatial interrelationships of the grey levels in a texture pattern and it is invariant under monotonic grey-level transformations. In general, a minimum set of co-occurrence matrices is four ($\phi = 0$, 45, 90 and 135°, respectively; $d = 1$) for the texture about which we have no prior knowledge. However, it is obvious that the size of the matrix is a function of the number of grey levels in the image, and it would be prohibitively expensive to evaluate matrix for each pixel in a general 8-bit image (256×256 elements in a co-occurrence matrix). Thus, we use the statistical parameter matrices with the same texture reservation properties, instead of the co-occurrence matrix.

The statistical method we adopted is 2-D autocorrelation, which can evaluate the texture parameters for several distances between pixels and directly from the image without using co-occurrence matrices. The main advantage of this method resides in its calculation cost, which depends only on the size of the image treated and not on the number of grey levels. Moreover, it allows the extraction of visually perceptible physical parameters from the image, such as contrast, granularity, regularity,

periodicity, finesse or coarseness of the texture, and so on.

The 2-D autocorrelation coefficients $A(\Delta m, \Delta n)$ between pixel (x, y) and pixel $(x + \Delta m, y + \Delta n)$ in an image with size $m \times n$ is defined as:

$$A(\Delta m,\Delta n) = \frac{1}{(m - \Delta m)(n - \Delta n)} \sum_{x=0}^{m-1-\Delta m} \sum_{y=0}^{n-1-\Delta n} f(x,y) \times f(x + \Delta m, y + \Delta n). \quad (9)$$

In general, Δm and Δn are set as the distances among pixels whose interrelationship is to be taken into consideration. Thus, there will be $\Delta m \times \Delta n$ coefficients. The autocorrelation contrast is then defined as the ratio of autocorrelation of inside the region and autocorrelation of the outside region. That is, the autocorrelation contrast is $A(\Delta m, \Delta n)_{\text{inside}} / A(\Delta m, \Delta n)_{\text{outside}}$.

Distribution distortion of wavelet coefficients

It has been shown that, for a large class of images, the transformed coefficients in each high-frequency subband can be well described by a generalized Laplacian distribution (Mallat 1989b), which is often simplified to the special case of Laplacian distribution (Chang et al. 1998). The Laplacian distribution *p(x)* is defined as:

$$p(x) = \frac{\lambda}{2} \cdot e^{-\lambda|x|}, \quad (10)$$

whose mean is zero and variance is $2/\lambda^2$. The histogram of HL subband wavelet coefficients of an image and Laplacian distribution is shown in Fig. 7. In this paper, the summation of differences among the real distribution of wavelet coefficients and the distribution of expected Laplacian distribution is adopted as our feature. That is, the distribution distortion of wavelet coefficients is defined as:

$$\sum_x |w(x) - p(x)|, \quad (11)$$

where *w(x)* is the real probability density function of the HL subband wavelet coefficients and *p(x)* is the expected Laplacian distribution.

The proposed three features are extracted synchronously in the wavelet decomposition stage. Variance contrast and autocorrelation contrast are extracted from the LL subband and the distribution distortion of wavelet coefficients is extracted from the HL subband.

Diagnosis

For differential diagnosis of breast tumors, we make use of the neural network trained by error backpropagation algorithm as our discriminating algorithm. To reduce the oscillation and training time during the training periods, the steepest descent with momentum is used in the training procedure (Looney 1997). It has been proven that an MLP neural network with one hidden layer performed well enough if the number of neurons in a MLP neural network was sufficient (Looney 1997). Hence, we use a MLP neural network with one hidden layer and trained by the error backpropagation algorithm with momentum as our discriminating method. The proposed three features are used as the inputs to neural network for diagnosing whether the tumor is benign or malignant. We find that the diagnosis procedure can precisely differentiate the breast tumors by using these three feasible features.

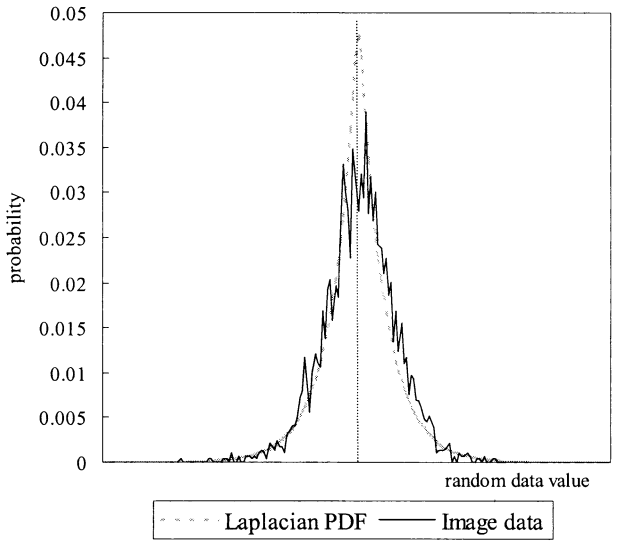

Fig. 7. Histogram for the HL subband wavelet coefficients and Laplacian probability density function.

RESULTS

The experimental results and performance evaluation of the proposed method are described in this section.

Data acquisition

The US breast image database we used was recorded from 1997 to 1998, and the ages of patients ranged from 17 to 64 years. All the images were captured from an ALOKA SDD 1200 scanner (Tokyo, Japan) and a 7.5-MHz linear real-time transducer with freeze-frame capability. No acoustic stand-off pad was used with any of the cases. The digital US images were obtained by transmitting the analog signals from the VCR output of the scanner to the frame grabber Video CATcher (Top Solution Technology; Taipei, Taiwan). Then, it digitized

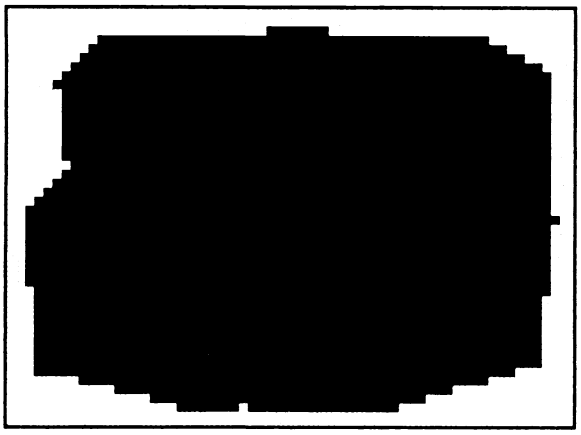

Fig. 8. The segmentation result of ROI image for Fig. 3. The black area indicates the tumor region and the white area indicates the surrounding tissues.

the data and generated frames of resolution 736 × 566 pixels for an NTSC (National Television Systems Committee) video-screen picture. The digital image was real-time captured and quantized into 8 bits (*i.e.,* 256 grey levels) using the Prolab's ProImage software package bundled with the frame grabber.

Experiment results

There were 242 breast digital US images of pathologically proven tumors, including benign breast tumors from 161 patients and carcinomas from 81 patients (either by cytology, core-needle biopsy or open biopsy) used in our study. All these breast images were captured by one surgeon (D. R. Chen, who is also familiar with breast US interpretations), who also selected the ROI; data were consecutively collected from 1997 to 1998. Patients' ages ranged from 17 to 64 years and tumor size measured from 0.8 to 4.2 cm.

The proposed segmentation algorithm is first applied on an ROI image to segment the tumor region from the surrounding tissues. Figure 8 shows the segmentation result of the ROI image in Fig. 3.

Next, we will concentrate on identifying the feasibility of three proposed features, variance contrast, autocorrelation contrast and distribution distortion of wavelet coefficients. We employed the three evaluated feature values of the 242 segmented ROI images to depict the histograms as benign or malignant, respectively. The histograms of the three features are shown in Figs. 9 to 11. It is easy to figure out that the malignant tumors are distributed with higher variance contrast values, lower autocorrelation contrast values and lower distribution distortion of wavelet coefficients values. In terms of the variation of histograms for benign and malignant tumors,

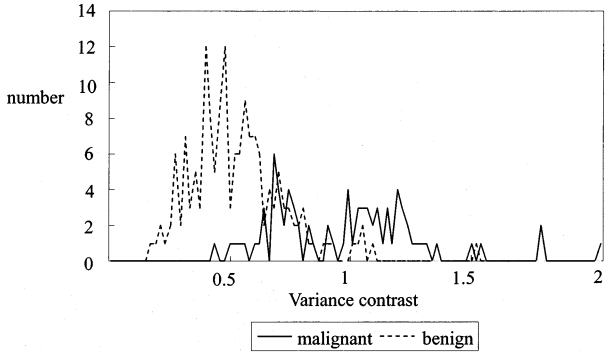

Fig. 9. Histogram of variance contrast.

we can make a conclusion that the three proposed features all have very good ability for classifying breast tumors.

Performance evaluation

In this study, the MLP neural network was adopted for differential diagnosis. The MLP neural network that we used is constructed by an input layer with three inputs, a hidden layer with six neurons and an output layer with one neuron. Three proposed features were used as the input values of the neural network. In the training procedure of MLP neural network, the decay (growth) rate α of the bipolar sigmoid performed on each neuron is 2.4. For each training epoch, the step gains η of the hidden layer and the output layer were 0.2 and 0.15, respectively. The activation function that we used for the neural network is simply a threshold value. All the cases with output values less than the threshold value were considered to be malignant, otherwise they were considered to be benign. The wavelet bases used in this paper for the wavelet transform was Daubechies with length 10.

The *k*-fold cross-validation method (Weiss and Kapouleas 1989) and the ROC curves (Egan 1975) were

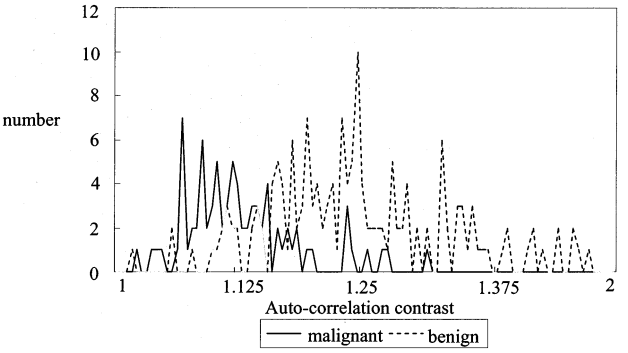

Fig. 10. Histograms of autocorrelation contrast.

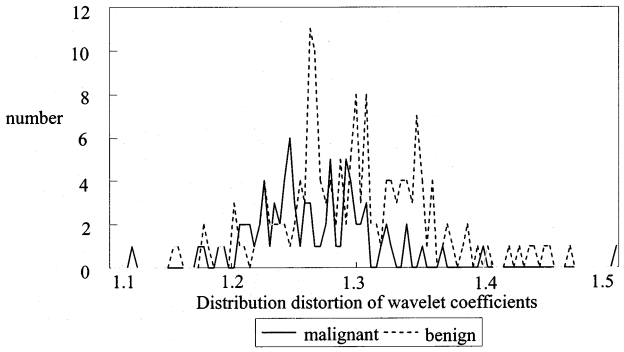

Fig. 11. Histograms of distribution distortion of wavelet coefficients.

used to evaluate the performance of our proposed method. First, we describe the *k*-fold cross-validation method as follows.

Step 1: The 242 images in the database were randomly divided into k groups $\{ G_1, G_2, \ldots, G_k \}$ and set $t = 1$.

Step 2: The group G_t was set aside, and the remaining (k –1) groups were used to train the neural network.

Step 3: The trained neural network was then tested on the group G_t that was set aside before.

Step 4: If $t = k$, then stop the process; otherwise, set $t = t + 1$, and go to step 2.

In our simulation, k was 10 and each group had 23 to 25 images. The simulation results of the divided 10 groups at threshold value $= -0.3$ are listed in Table 1.

Sensitivity, specificity, positive predictive value and negative predictive value are the most generally used objective indices to estimate the performance of diagnosis results. The four indices are defined as follows.

Sensitivity = TP/(TP+FN)

Specificity = TN/(TN+FP)

Positive predictive value = TP/(TP+FP)

Negative predictive value = TN/(TN+FN)

The definition of TP, TN, FP and FN are specified as follows:

Table 1. The number of misdiagnosed cases for each test set at threshold value $= -0.3$

Test set	Malignant cases	Benign cases
1	0 of 8	1 of 16
2	0 of 7	3 of 16
3	0 of 8	3 of 16
4	0 of 8	1 of 16
5	0 of 8	5 of 16
6	1 of 8	4 of 16
7	0 of 8	3 of 16
8	0 of 8	4 of 17
9	0 of 9	3 of 16
10	0 of 9	3 of 16

Table 2. The performance for different threshold values of the activation function

Threshold	Sensitivity	Specificity	FN	FP
−1	1.0000	0.0000	0	161
−0.9	1.0000	0.4596	0	87
−0.8	1.0000	0.5776	0	68
−0.7	0.9877	0.6832	1	51
−0.6	0.9877	0.7267	1	44
−0.5	0.9877	0.7826	1	35
−0.4	0.9877	0.8137	1	30
−0.3	0.9877	0.8137	1	30
−0.2	0.9630	0.8199	3	29
−0.1	0.9630	0.8323	3	27
0	0.9506	0.8323	4	27
0.1	0.9383	0.8323	5	27
0.2	0.9259	0.8385	6	26
0.3	0.9012	0.8509	8	24
0.4	0.8642	0.8634	11	22
0.5	0.8642	0.8820	11	19
0.6	0.8519	0.9006	12	16
0.7	0.8148	0.9193	15	13
0.8	0.7037	0.9317	24	11
0.9	0.5432	0.9565	37	7
1	0.0000	1.0000	81	0

TP (true-positive): the number of correctly diagnosed malignant cases

TN (true-negative): the number of correctly diagnosed benign cases

FP (false-positive): the number of incorrectly diagnosed benign cases

FN (false-negative): the number of incorrectly diagnosed malignant cases

Among the four performance indices, sensitivity and specificity are the most important values with which a doctor is concerned. Table 2 shows the simulation results of these two performance indices using different threshold values for the activation function of MLP neural network. The overall performance for the threshold value −0.3 is listed in Table 3. Table 4 shows the overall performance of our proposed method and the standard linear classifier (Therrien et al. 1989). The experienced radiologists, Stavros et al. (1995) and Skaane and Engedal (1998) reported that the sensitivities of breast US

Table 3. The overall performance at threshold value −0.3 for the activation function

	Benign	Malignant
Output $<$ −0.3	TN 131	FN 1
Output $>$ −0.3	FP 30	TP 80
Total	161	81

Sensitivity = 80/(80+1) = 98.77%; Specificity = 131/(131+30) = 81.37%; Positive predictive value = 80/(80+30) = 72.73%; Negative predictive value = 131/(131+1) = 99.24%.

Table 4. The overall performance between proposed method and the standard linear classifier

	Proposed method, %	Standard linear classifier %
Sensitivity	98.77	93.83
Specificity	81.37	83.23
Positive predictive value	72.73	73.79
Negative predictive value	99.24	96.40

for malignancy were 98.4% and 99.55%, the specificities were 67.8% and 29%, the positive predictive values were 38% and 66% and the negative predictive values were 99.5% and 98%, respectively; the overall accuracy as reported by Stavros et al. (1995) was 72.9%. Current procedures for detecting and diagnosing breast cancers, however, illustrate the difficulty in maximizing both sensitivity and specificity. With a sensitivity of 98.77% and a specificity 81.37%, our proposed method provides objective evidence for good diagnoses of breast tumors.

The ROC curve was evaluated from false-positive fraction (FPF) and true-positive fraction (TPF). The FPF indicates the fraction of FP and total number of benign cases. The TPF indicates the fraction of TP and total number of malignant cases. ROC curve is depicted based on the statistical decision theory and estimated from all of the decision thresholds. From the ROC curve, we could clearly figure out the trade-off between FPF and TPF. In general, the thresholds with higher TPF are adopted to avoid the case that malignant tumors were misdiagnosed. The ROC area index A_z is usually used as a measure of overall performance for the neural network classification. The ROC curve of the proposed method is depicted in Fig. 12. It shows that the A_z value of our method is high, with the value 0.9396 ± 0.0183 (SD).

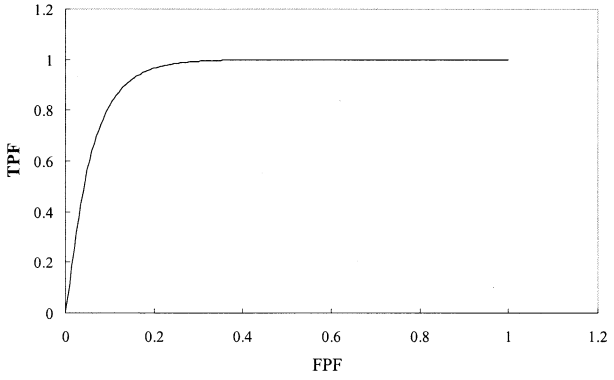

Fig. 12. The diagram of the ROC curve for our proposed method with A_z value 0.9396 ± 0.0183.

DISCUSSION

In this paper, we proposed a novel diagnosis system for differentiating breast tumors. First, the segmentation algorithm is applied in ROI image to segment the tumor region from the surrounding tissues. Three feasible features, variance contrast, autocorrelation contrast, and distribution distortion of wavelet coefficients, which exhibit outstanding representation for differentiating tumors are then proposed. With the three features, the MLP neural network trained by the error-backpropagation with momentum differentiated the tumors into benign and malignant cases correctly. This study further demonstrates the potential of image texture analysis as an important component of CAD algorithms, and that the combination of image texture analysis and automatched decision-making offers a promising approach to a clinical challenge.

In the previous report by Garra et al. (1993), the feature of the ROI that covers the tumor is better than the feature of the ROI that lies completely within the tumor boundary. In our recent study (Chen et al. 2000), the diagnostic performances were better using the ROI outside the tumor than inside the tumor, either in longitudinal or transverse scanning planes. The drawback in the ROI selection by Garra and colleagues and our previous method was that ROI was manually selected with a region that extended beyond the lesion margins by 1 to 2 mm in all directions. However, the region selection was inconsistent. But, in clinical practice, it is inconvenient to use an ROI that lies completely along the tumor boundary. To draw a rectangular region in the computer is an easy and quick way for most applications. One of the contributions of this study is that it applied the segmentation algorithm to segment the tumor region from the surrounding tissues to get a consistent ROI, and we believe this can be expected to improve interpretative accuracy. Furthermore, this is an important step toward the autodiagnosis for the future CAD system.

REFERENCES

Averbuch LD, Israeli M. Image compression using wavelet transform and multiresolution decomposition. IEEE Trans Image Processing 1996;5:4–15.

Antonini M, Barlaud M, Mathieu P, Daubechies I. Image coding using wavelet transform. IEEE Trans Image Processing 1992;1:205–220.

Bassett LW, Liu TH, Giuliano AT, Gold RH. The prevalence of carcinoma in palpable vs impalpable, mammographically detected lesions: The value of sonographic texture analysis. J Ultrasound Med 1993;13:267–285.

Boring CC, Squires TS, Tong T, Montgomery S. Cancer statistics, 1994. CA Cancer J Clinicians 1994;44:7–26.

Chang SG, Yu B, Vetterli M. Multiple copy image denoising via wavelet thresholding. Proceedings of the IEEE International Conference on Image Processing, 1998545–549.

Chang T, Kao CJ. Texture analysis and classification with tree-structured wavelet transform. IEEE Trans Image Processing 1993;2: 429–441.

Chen DR, Chang RF, Huang YL, et al. Texture analysis of breast tumors on sonograms. Semin Ultrasound CT MRI 2000;21:308–316.

Chou YH, Tiu CM, Hung GS, et al. Stepwise logistic regression analysis of tumor contour features for breast ultrasound diagnosis. Ultrasound Med Biol 2001;27:1493–1498.

Dhawan P, Chitre Y, Kaiser-Bnoasso C, Moskowitz M. Analysis of mammographic microcalcifications using gray-level image structure features. IEEE Trans Med Imaging 1996;15:246–259.

Egan JP. Signal detection theory and ROC analysis. New York: Academic Press, 1975.

Freer Tw, Ulissey MJ. Screening mammography with computer-aided detection: Prospective study of 12,860 patients in a community breast center. Radiology 2001;220:781–786.

Garra S, Krasner BH, Horii SC, et al. Improving the distinction between benign and malignant breast lesions: The value of sonographic texture analysis. J Ultrasound Med 1993;13:267–285.

Gisvold JJ, Martin JJ. Prebiopsy localization of nonpalpable breast lesions. AJR 1984;143:477–481.

Hirose Y, Yamashita K, Hijiva S. Back-propagation algorithm which varies the number of hidden units. Neural Networks 1991;4:61–66.

Jiang Y, Nishikawa RM, Schmidt RA, et al. Potential of computer-aided diagnosis to reduce variability in radiologist's interpretations of mammograms depicting microcalcifications. Radiology 2001; 220:787–794.

Looney CG. Pattern eecognition using neural networks. Oxford: Oxford University Press, 1997.

Mallat SG. Multifrequency channel decompositions of images and wavelet models. IEEE Trans Acoust Speech Signal Processing 1989a;37:2091–2110.

Mallat SG. A theory for multiresolution signal decomposition: The wavelet representation. IEEE Trans Pattern Anal Mach Intell 1989b;11:674–693.

Petrick N, Chan HP, Sahiner B, Wei D. An adaptive density-weighted contrast enhancement filter for mammographic breast mass detection. IEEE Trans Med Imag 1996;15:59–67.

Richardson WB Jr. Applying wavelets to mammograms. IEEE Eng Med Biol Mag 1995;14:551–560.

Rosenberg L, Schwartz GF, Feig SA, Patchefsky AS. Clinical occult breast lesions; localization and significance. Radiology 1987;162: 167–170.

Rumelhart DE, Hinton GE, Williams RJ. Learning representation by back-propagation errors. Nature 1986;323:533–536.

Sahiner B, Chan HP, Petrick N, et al. Classification of mass and normal breast tissue: A convolution neural network classifier with spatial domain and texture images. IEEE Trans Med Imag 1996;15:598–610.

Shankar PM, Reid JM, Ortega H, et al. Use of non-Rayleigh statistics for identification of tumors in ultrasonic B-scans of the breast. IEEE Trans Med Imaging 1993;12:687–692.

Skaane P, Engedal K. Analysis of sonographic features in the differentiation of fibroadenoma and invasive ductal carcinoma. AJR 1998;170:109–114.

Stavros T, Thickman D, Rapp CL, et al. Solid breast nodules: Use of sonography to distinguish between benign and malignant lesions. Radiology 1995;196:123–134.

Therrien CW. Decision, estimation, and classification: An introduction to pattern recognition and related topics. New York: Wiley, 1989.

Weiss SN, Kapouleas I. An empirical comparison of pattern recognition neural nets and machine learning classification methods. Proceedings of the 11th International Joint Conference on Artificial Intelligence, 1989:234–237.

Zheng BY, Qian W, Clarke LP. Digital mammography: Mixed feature neural network with spectral entropy decision for detection of microcalcifications. IEEE Trans Med Imaging 1996;15:589–597.